J. For. Res. (2017) 28(2):215–229
DOI 10.1007/s11676-016-0361-8

REVIEW ARTICLE

The progress of operational forest fire monitoring with infrared remote sensing

Lizhong Hua[1] · **Guofan Shao**[2]

Received: 12 October 2016 / Accepted: 22 November 2016 / Published online: 17 December 2016

Abstract Forest wildfires pose significant and growing threats to human safety, wildlife habitat, regional economies and global climate change. It is crucial that forest fires be subject to timely and accurate monitoring by forest fire managers and other stake-holders. Measurement by space-borne equipment has become a practical and appealing method to monitor the occurrence and development of forest wildfires. Here we present an overview of the principles and case studies of forest fire monitoring (FFM) with satellite- and drone-mounted infrared remote sensing (IRRS). This review includes four types of FFM-relevant IRRS algorithms: bi-spectral methods, fixed threshold methods, spatial contextual methods, and multi-temporal methods. The spatial contextual methods are presented in detail since they can be applied easily with commonly available satellite IRRS data, including MODIS, VIIRS, and Landsat 8 OLI. This review also evaluates typical cases of FFM using NOAA-AVHRR, EOS-MODIS, S-NPP VIIRS, Landsat 8 OLI, MSG-SEVIRI, and drone infrared data. To better implement IRRS applications in FFM, it is important to develop accurate forest masks, carry out systematic comparative studies of various forest fire detection systems (known as forest fire products), and improve methods for assessing the accuracy of forest fire detection. Medium-resolution IRRS data are effective for landscape-scale FFM, and the VIIRS 375 m contextual algorithm and RST-FIRES algorithm are helpful for closely tracking forest fires (including small and short-lived fires) and forest-fire early warning.

Keywords Landsat 8 OLI · MODIS · Remote sensing · Review · Thermal infrared · VIIRS · Wildfire

Introduction

Forest wildfires threaten human safety, wildlife habitat, regional economies, and global climate change (Martell 2015) in addition to ecosystem structure and nutrient cycling (Roy et al. 2008). As an important source of aerosols and greenhouse gas emissions in several regions of the world, forest fires affect local air quality, atmospheric chemistry, and weather (Pozo et al. 1997; Vadrevu et al. 2015; Li et al. 2015). Globally over 200,000 wildfires occur annually, burning a total land area of 3.5–4.5 million km^2, which is equivalent to 1/3–1/2 of the land area of China, United States or Canada (Meng et al. 2015). Furthermore, severe forest wildfire incidents have been increasing in many parts of the world (e.g., western United States), and such a growing and dangerous trend has elevated both public and political awareness (Andreae 2013; Dennison et al. 2014).

Early and accurate detection and monitoring of forest fires are critically important for resource managers who

Project funding This research was financially supported by The National Natural Science Foundation of China [41471366] and The McIntire-Stennis Cooperative Forestry Research Program.

The online version is available at http://www.springerlink.com

Corresponding editor: Chai Ruihai

✉ Guofan Shao
shao@purdue.edu

Lizhong Hua
lzhua@xmut.edu.cn

[1] College of Computer and Information Engineering, Xiamen University of Technology, Xiamen 361021, China

[2] Department of Forestry and Natural Resources, Purdue University, 715 West State Street, West Lafayette, IN 47907, USA

want to reduce the potential damages and costs of fire suppression (Qu et al. 2008; Ahmad 2014). It is necessary to collect quantitative information about the spatiotemporal extent of forest fires for better forest management, wildlife protection, and atmospheric chemistry monitoring (Li et al. 2000; Pu et al. 2004). Prior to the availability of computerized geospatial technologies, forest fires were monitored by patrols at fire lookout towers and sometimes by campers, hikers, and rangers on the ground (Weaver et al. 1995). In the past four decades, spaceborne remote sensing systems and wireless sensor networks have emerged. Ground automatic detection systems have been widely developed by using optical camera sensors on towers and buildings (San-Miguel-Ayanz and Ravail 2005). Crewed airborne techniques have been replaced by unmanned aerial systems (UAS) or drones to ensure the safety of fire observers (Tang and Shao 2015). All of these techniques have been applied in forest fire monitoring (FFM). Wireless sensor network (WSN) is a promising method that might be used in FFM to further support real-time fire-control tactics, but its application is still in its infancy. Researchers also experiment in FFM by using the methods of light detection and ranging (LIDAR) (Lavrov et al. 2006) and radio-acoustic sounding (Sahin and Ince 2009). Among the existing FFM methods, remote sensing has unique advantages because it can provide data at lower costs, larger spatial scales, and higher acquisition frequencies, all of which are critical for real-time FFM.

FFM at regional and global scales is commonly achieved by using sensors on earth-observation satellites (Giglio et al. 2006). This remote sensing technique has been applied to identify active forest fires, predict fire propagation potential, monitor the burned area, examine spatiotemporal patterns of fire intensity, and assess forest wildfire risk in different regions (Meng et al. 2015). Remote sensing-based FFM can be achieved through the uses of polar-orbiting or geostationary satellites (Table 1). Polar-orbiting sensors offer finer spatial resolution ($\leq$1 km) and thus improve detection of smaller and lower intensity fires, while enhancing the precision of descriptions of their locations (Schroeder et al. 2008). In the last three decades, many long-term and regional/global-scale FFM studies were based on the advanced very high resolution radiometer (AVHRR) onboard the National Oceanic and Atmospheric Administration (NOAA) satellite (Flannigan and Haar 1986; Kaufman et al. 1990; Kennedy et al. 1994; Li et al. 2000; Gong et al. 2006) as well as track scanning radiometer (ATSR) and the advanced-ATSR (AATSR) onboard European remote sensing (ERS) satellites (Arino and Rosaz 1999), the visible and infrared scanner (VIRS) onboard the tropical rainfall measuring mission (TRMM) satellite, the Moderate resolution imaging spectroradiometer (MODIS) onboard the earth

Table 1 Characteristics of the main sensors used in fire monitoring algorithms

Characterizations of the sensors	AVHRR		Terra/Aqua MODIS		VIIRS 750		VIIRS 375		Landsat 8 OLI		SEVIRI	
Channels	C#	SR (μm)	C#	SR (μm)	C#	SR (μm)	C#	SR (μm)	C#	SR (μm)	C#	SR (μm)
	3	3.55–3.93	**21**	3.929–3.989	**M13**	3.973–4.128	**I4**	3.550–3.930	**5**	0.85–0.88	**4 (IR3.9)**	3.48–4.36
	4	10.30–11.30	**31**	10.78–11.28	**M15**	10.263–11.263	**I5**	10.500–12.400	**7**	2.11–2.29	**9(IR10.8)**	9.80–11.80
ST-MIR (K)		325		500		634		367				
Spa-Res (m)		1100		1000		750		375		30		3000
Swath width (km)		2399		2330		3040		3040		185		
Revisit cycle		Visible data daily; infrared imaging twice daily		At least twice daily for each satellite		12 h		12 h		16 days		≤15 min
Active fire products availability		1998–current		2001-current		2012–current		2016–current		2015–current		2007–current

C# channel number, *SR* spectral range, *ST-MIR* saturation temperature in middle thermal infrared channel, *Spa-Res* spatial resolution. Channel number in bold means key channels to detect active fire in each algorithm

observation satellites (EOS) terra and aqua (Giglio et al. 2003), and more recently the visible infrared imaging radiometer suite (VIIRS) onboard the Suomi-National Polar-orbiting Partnership (S-NPP) satellite (Schroeder et al. 2014) and Operational Land Imager (OLI) onboard Landsat-8 (Loveland and Irons 2016; Schroeder et al. 2016). However, their temporal resolution (>hours) is not high enough for detecting short-lived events or fires characterized by a marked diurnal cycle and rapid evolution times (Schroeder et al. 2016). In contrast, geostationary sensors operating above the equator have coarser spatial resolution but provide higher frequently observation of the surface than do polar orbiting sensors. Geostationary satellites include the US geostationary operational environmental satellites (GOES), Europe meteosat second generation (MSG), and China Fēngyún (FY), which are suitable for near-real time fire monitoring as they give continuous data over the same position on Earth within a short period of time. Their limitations are that they cannot easily sense high-latitude regions.

We searched for relevant ISI publications with the keywords "forest fire monitoring" and any of "AVHRR, MODIS, VIIRS, SEVIRI and Landsat 8 OLI or drone" from the website of Science TM Core Collection as of December 2015, resulting in a total of 322 papers (Fig. 1). The first publication was based on AVHRR data in 1986 but AVHRR applications in FFM have declined since 2005. Since 1992, the total number of FFM-remote sensing publications has greatly increased. Among the five satellite sensors and drone remote sensing, MODIS data were used most frequently (46.9%) followed by AVHRR (35.1%) and drones (7.1%) (Fig. 1). The Landsat 8-OLI and VIIRS with higher resolutions have been applied in FFM since 2013. The results of our literature review suggest that the research interest in FFM has been increasing and a broad range of infrared remote sensing (IRRS) methods have been applied in FFM.

The purpose of this review is to evaluate the effectiveness of the major sensors and algorithms for FFM, and to discuss the limitations and strengths of these approaches. The critical cases of FFM with the five satellite sensors and one drone sensor are introduced and summarized. The future directions of FFM with IRRS are discussed.

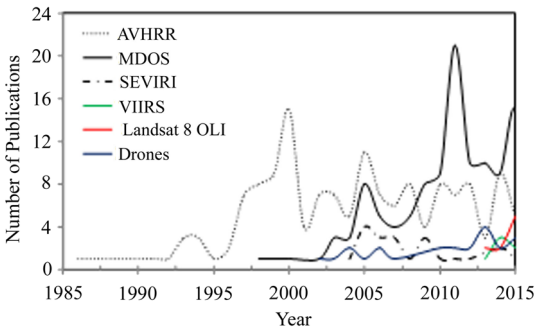

Fig. 1 Comparisons of published items change trends for five satellite sensors and one drone remote sensing from 1985 to 2015

Physical principles of fire detection

The procedure of forest fire detection is mainly based on the middle infrared (MIR) (3–5 μm) and thermal infrared (TIR) (8–14 μm) channels of remote sensing imagery. The principles of forest fire detection are based mainly on the laws of Planck, Wien's displacement, and Stefan-Boltzmann (Calle and Casanova 2008). The wavelength of maximum blackbody radiances decreases with increasing temperature (Fig. 2). For example, a blackbody with a temperature of 300 K has its peak radiative energy at ~10 μm; a blackbody with a temperature of 500–800 K (typical forest fires) has its peak radiative energy at 3–5 μm. Furthermore, for a given increase in temperature, the radiation of the MIR channel increases more rapidly than that of the TIR channel. For instance, an increase in temperature from 500 to 800 K will lead to an increase in thermal radiation from 82 to 682 W m^{-2} μm^{-1} sr^{-1} at the 4 μm channel, but the radiation only increases from 58 to 135 W m^{-2} μm^{-1} sr^{-1} at the 11 μm channel. Therefore, not only the temperature values of fire pixels in the MIR channel are significantly greater than those in the TIR channel, but also the MIR channel is more sensitive to fire pixels than is the TIR channel. This physical theory is the foundation for fire detection approaches using IRRS. Matson and Dozier (1981) and Dozier (1981) first proposed a method to estimate the sub-pixel fire temperature and area using information from two or more infrared channels based on the concepts of the Planck radiance function. Since then, a variety of IRRS data collected by spaceborne

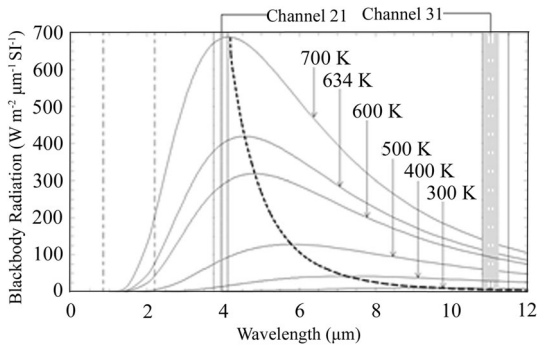

Fig. 2 Planck function showing blackbody emission with different temperatures source and locations of MODIS channels 21 and 31, and location of central wavelength of AVHRR 3.75–10.80-μm channel (*vertical dash lines*), VIIRS 750 m 4.128-, 11.5-μm channels (*vertical solid lines*), Landsat 8 OLI 0.86-, 2.20-μm channel (*vertical dot-dashed lines*)

or airborne equipment, have been routinely used for detecting and monitoring forest fires.

Commonly used IRRS for FFM

NOAA-AVHRR

AVHRR is one of the primary sensors onboard the NOAA satellite. AVHRR-2 with a 5-channel radiometer was initially carried on NOAA-7 launched in 1981. It was later improved to a 6-channel instrument (AVHRR-3) carried on NOAA-15 launched in 1998. Currently, the newest AVHRR data are transmitted from the operational satellite, NOAA-19, launched in 2009. This radiometer uses six detectors that collect different bands of radiation wavelengths, including one MIR band and one TIR band (Table 1). NOAA satellite imagery has a high temporal resolution of 12 h revisiting time.

AVHRR was designed mainly for weather surveillance and monitoring of sea surface temperatures. A major limitation of the AVHRR sensor for fire characterization was its low saturation of about 325 K at its MIR channel (band 3), which precluded distinction between small and large fires and between smoldering and flaming fires (Kaufman et al. 1998). Despite this weakness, AVHRR provided a broad base of experience for satellite detection of vegetation fires. As a pioneer sensor for exploring the performance of fire detection, AVHRR data from fire studies guided development of MODIS fire product (FP) needs and design.

An active FP developed from AVHRR, namely fire identification, mapping and monitoring algorithm (FIMMA), was released by NOAA satellite service division. FIMMA was based on modifications of the fire detection algorithms proposed by Li et al. (2000, 2001) and Giglio et al. (1999). FIMMA was relatively accurate in forested regions but could fail to detect fires in urban and agricultural regions.

Terra/aqua MODIS

MODIS instruments onboard Terra and Aqua polar orbiting satellites were launched as part of NASA's Earth Observing System in 1999 and 2001, respectively. MODIS was intended to monitor global fire activity up to four observations in 24 h (Kaufman et al. 1998). By using a special fire channel >3.9 μm that is influenced less by solar reflection than is the <3.9 μm channel used by AVHRR (Table 1), MODIS has a great advantage in FFM over AVHRR. Other advantages include high positional accuracy, high temporal resolution, high radiometric resolution, and high spectral resolution (Kaufman et al. 1998).

Kaufman et al. (1998) first developed a fire monitoring algorithm for MODIS data and created the MODIS Collection 3 (MODIS C3) FP, which marked a milestone in the development of fire monitoring with remote sensing due to its high spectral and spatial resolutions (Kaufman et al. 1998). The MODIS C3.0 algorithm has been refined several times to generate new MODIS FPs with better performance (Giglio et al. 2003, 2016).

S-NPP VIIRS

VIIRS instruments onboard the S-NPP satellite began collecting data in 2011. VIIRS provides significant enhancements to environmental monitoring (such as wildfires and land-use changes) and numerical weather forecasting, with a 22-band radiometer covering wavelengths including a MIR channel of 3.973–4.128 μm. VIIRS imagery has a 3040 km swath width and provides twice daily global coverage (Cao et al. 2014).

VIIRS provides data at two spatial resolutions of 750 and 375 m, improving upon the existing moderate-to-coarse resolution sensors. In addition, VIIRS also improved spatial sampling with a specific pixel aggregation scheme. This unique scheme not only eliminates coverage gaps over lower latitudes and minimizes increases in pixel size with scan angle, but also provides consistent performance for daily mapping of fires lasting several days (Csiszar et al. 2014; Schroeder et al. 2014).

Currently, two FPs have been developed using VIIRS data: one at 750 m (Csiszar et al. 2014) and one at 375 m resolution (Schroeder et al. 2014). VIIRS has higher spatial resolution and is capable of detecting smaller fires at nadir than is MODIS (Blackett 2015).

Landsat 8-OLI

Landsat-8 was launched in 2013 carrying the OLI and the Thermal Infrared Sensor (Loveland and Irons 2016) with a 16-day repeat cycle (Table 1). The OLI sensor has eight spectral channels with a spatial resolution of 30 m plus a 15 m panchromatic channel. Landsat-8 active fire detection was based on previous algorithms developed for the Advanced Spaceborne Thermal Emission and Reflection Radiometer (ASTER) and Landsat-7 ETM+ (Giglio et al. 2008; Schroeder et al. 2008). Since Landsat 8 lacks ~4 and 11 μm channels, the algorithm was driven by the fire-sensitive SWIR channel 7 (2.20 μm) and channel 5 (0.86 μm) (Schroeder et al. 2016). The Landsat 8 OLI has much higher spatial resolution than does VIIRS and is expected to detect smaller fires at nadir than can VIIRS.

MSG-SEVIRI

The Spinning Enhanced Visible and Infrared Imager (SEVIRI) is one of the primary sensors onboard MSG satellites. The MSG-1 satellite was launched in 2002. The latest satellite of the MSG series, MSG-4 (i.e., Meteosat-10), was launched in 2015. SEVIRI observes the earth with improved performance compared to its Meteosat predecessors. With 12 channels, i.e. 11 narrow-bandwidth channels with 3 km resolution at nadir and one high-resolution broad-bandwidth channel with 1 km resolution, and very high temporal resolution, SEVIRI has a higher probability of detecting short-lived fires, small fires, and fires with strong diurnal cycles (Table 1). With a temporal resolution from 15 to 5 min, the SEVIRI sensor benefits European countries (mainly southern Europe) that often suffer from short-duration fires between 12:00 and 14:00 o'clock local time.

Fire-detection methods based on multi-temporal analyses are especially suitable for MSG-SEVIRI because the SEVIRI sensor operates under stable observational conditions at the pixel level, including fixed view angles, same time of day, and same ground resolution (Filizzola et al. 2016). Numerous algorithms have been developed for SEVIRI data, including fixed threshold or contextual algorithms (Roberts and Wooster 2008), and multi-temporal change detection analyses, such as the Kalman filter approach (Roberts and Wooster 2014) and robust satellite techniques (RST) for FIRES detection and monitoring (RST-FIRES) (Filizzola et al. 2016).

Drone IRRS

Drones are also known as unmanned aerial vehicles (UAV) or UAS. Drone platforms can be divided into two major types, fix-wing and rotary-wing drones, according to their takeoff and landing techniques. The former type is suitable for a large field coverage while the latter may be superior for recording high spatial resolution measurements (Tang and Shao 2015). Drones can be equipped with a number of sensing instruments, ranging from optical sensors (including visible and infrared) to microwave sensors (Radar and Lidar) (Shao 2015). The uses of drones in FFM have drawn much attention in recent years (Merino et al. 2012; Ollero and Merino 2006). Owing to their flexibility and low cost, and high resolution data collection, drone remote sensing can fill data gaps and supplement the capabilities of manned aircraft and satellite remote sensing systems while reducing the risks associated with manned aircraft flying near fires (Tang and Shao 2015).

IRRS algorithms for FFM

Many IRRS algorithms have been developed for regional or global fire detection and monitoring (e.g., Kaufman et al. 1998; Giglio et al. 2003; Wang et al. 2007). Methods can be divided into four broad categories: bi-spectral methods, threshold methods, spatial contextual methods and multi-temporal fire detection methods.

Bi-spectral methods

Bi-spectral methods were originally proposed by Dozier (1981) to determine a sub-pixel fire temperature and instantaneous area using the MIR and TIR channels of AVHRR (Kaufman et al. 1998). In the model, a pixel contained a hot target of uniform temperature that occupied a fraction (from 0 to 1) of the pixel. The method can apply the spectral contrast between a sub-pixel fire hot-spot and the surrounding (presumably uniform) background area of the pixel for both channels. The method used the following two equations to solve for the fire temperature (T_f) and the fractional area of the pixel covered by fire (p, $0 < p < 1$).

$$L_4 = pB(\lambda_4, T_f) + (1-p)B(\lambda_4, T_b) \quad (1)$$

$$L_{11} = pB(\lambda_{11}, T_f) + (1-p)B(\lambda_{11}, T_b) \quad (2)$$

where, L_4 and L_{11} are radiances in the MIR (λ_4) and TIR (λ_{11}) channels; $B(\lambda, T)$ is the Planck function; T_b is the radiant (not kinetic) temperature of the non-fire background.

The original Dozier method was proposed for AVHRR data but could be applied to data from any sensors such as MODIS with similar MIR and TIR channels (Peterson et al. 2013). The Dozier method was built on a series of assumptions (Giglio and Kendall 2001; Li et al. 2001): (1) both the fire and background pixel were homogeneous temperature fields; (2) atmospheric effects were neglected; and (3) pixels were not saturated in both channels. These assumptions limited the applicability of this approach.

Several studies modified the algorithm to create a more realistic retrieval, such as bi-spectral infrared detection (BIRD) (Zhukov et al. 2006) and multiple endmember spectral mixture analysis (MESMA) (Eckmann et al. 2008). As a result, the uses of the bi-spectral methods have grown rapidly (Flannigan and Haar 1986; Langaas 1992; Peterson, et al. 2013; Giglio and Schroeder 2014). Giglio and Schroeder (2014) introduced a widely used improved bi-spectral method, which can be expressed using the following equations.

$$L_4 = \tau_4 pB(\lambda_4, T_f) + (1-p)L_{b,4} \quad (3)$$

$$L_{11} = \tau_{11} pB(\lambda_{11}, T_f) + (1-p)L_{b,11} \quad (4)$$

where, τ_4 and τ_{11} are the band-weighted atmospheric transmittances; $L_{b,4}$ and $L_{b,11}$ are the top-of-atmosphere MIR and TIR radiance contributions of the non-fire background in each channel, which can be estimated by averaging the radiance of neighboring fire-free pixels.

This improved method includes the atmospheric effects and the solar reflective contribution of small surfaces in daytime images.

Threshold methods

The threshold techniques (e.g., Arino and Melinotte 1998; Li et al. 2000) regards a pixel as fire if the brightness temperature in one or more spectral channels exceeds the predefined thresholds. The algorithms could be classified into two categories: single-channel threshold (SCT) and multi-channel threshold (MCT) algorithms (Li et al. 2001).

SCT algorithm

The SCT algorithm relies only on bright temperature in the MIR channel, denoted by T_4, (e.g., the AVHRR 3.75 μm or MODIS 3.96 μm channel) (Li et al. 2001). The algorithm detects a fire (hot spot) if a pixel temperature T_4 is greater than a pre-defined threshold.

The algorithm was faced with a great challenge to detect fires during daytime because solar reflection from bright objects (e.g., cloud and bare surfaces) had dramatic impact on fire detection using the MIR channel at low saturation limits. It was recommended that bright objects be eliminated prior to using the method, in order to increase the effectiveness of the MIR channel threshold (Li et al. 2001). The SCT algorithm was more effective for the evening satellite overpasses and thus the contribution from reflected sunlight was minimal (Langaas 1992) though the sources of heat such as industries or refineries can still lead to errors in fire detection. The method was also especially useful for detecting fires in relatively cool environments and regions with low solar reflectivity (Setzer and Pereira 1991).

MCT algorithms

The MCT method partially overcame the difficulty of the SCT method. The MCT techniques (e.g., Kaufman et al. 1990; Kennedy et al. 1994) used multiple observations in MIR and TIR channels and were based on the fact that high temperature sources produce a high MIR signal but have little effect on the TIR channel. The MCT algorithms consisted of three basic steps and tests (Kaufman et al. 1990; Li et al. 2001): (1) using T_4 to identify all potential fires ($T_4 > T_{\text{threshold1}}$); (2) using brightness temperature in TIR channel, denoted by T_{11}, (e.g., AVHRR 10.8 μm or MODIS 11.0 μm channel) to eliminate clouds ($T_{11} > T_{\text{threshold2}}$); and (3) using the difference between brightness temperature in MIR and TIR channels (denoted by ΔT) to remove false fires from warm background ($\Delta T = T_4 - T_{11} > T_{\text{threshold3}}$). In addition to these three basic tests, additional tests might also be applied, in particular for coping with reflective surfaces and different types of clouds (Li et al. 2000, 2001).

The advantage of the MCT method was its computational simplicity. The limitation was that the MCT are applicable only at local to regional scales during a short fire season (Pu et al. 2004). These simple values are often inadequate when applied to heterogeneous, or simply different, geographical areas or seasons. Various degrees of success in fire detection have been achieved using the MCT method when it was applied over wide homogeneous areas, tropical forests (Kaufman et al. 1990), boreal areas (Li et al. 2000) and savannahs (Kennedy et al. 1994; Cuomo et al. 2001). Another disadvantage of MCT was that it produced too many false alarms (Cuomo et al. 2001; Pu et al. 2004).

Most of the extant fire detection algorithms that were developed for regional applications have been tuned accordingly though they adopted similar processing steps and input data (Giglio et al. 1999). Table 2 summarizes the thresholds for four MCT methods. Two of them were developed and employed by the Canadian Center for Remote Sensing (Li et al. 2000) and the European Space Agency (Arino and Melinotte 1998).

Spatial contextual methods

Spatial contextual algorithms detect fire-affected pixels by comparing the 'background' brightness temperatures measured in neighboring pixels assumed to be unaffected by fire (Giglio et al. 2003). This approach partially compensated for some of the problems resulting from SCT and MCT methods (Filizzola et al. 2016).

Fire detection procedure based on spatial contextual methods typically consisted of three basic stages: determining preliminary thresholds to identify potential fire pixels, performing contextual tests to confirm fires among the potential fire pixels (Li et al. 2001), and setting thresholds to reject false alarms.

A series of contextual algorithms has been developed and applied widely to generate globally active FPs for different satellite sensors such as MODIS, VIIRS (Schroeder et al. 2014) and Landsat-8 OLI (Schroeder et al. 2016). Among these, MODIS FPs are the most mature since they were generated based on a number of improved algorithms such as MODIS Collection 3 (Kaufman et al. 1998), Collection 4 (Giglio et al. 2003), Collection 5, and Collection 6 (Giglio et al. 2016) (denoted by C3, C4, C5,

Table 2 Summary of four major multi-channel threshold algorithms using AVHRR data

Algorithm description	CCRS Li et al. (2000)	ESA Arino and Melinotte (1998)	Kaufman et al. (1990)	Kennedy et al. (1994)
Algorithm geographic applicability	Canada	Global/regional	Brazil	West Africa
Potential fire detection	$T_4 > 315$	$T_4 > 320$	$T_4 \geq 316$	$T_4 \geq 320$
Eliminate hot surfaces/warm background	$\Delta T \geq 14$	$\Delta T > 15$	$\Delta T \geq 10$	$\Delta T \geq 15$
Eliminate cold clouds	$T_{11} \geq 260$	$T_{11} > 245$	$T_{11} \geq 250$	$T_{11} \geq 295$
Eliminate cloud edges or thin clouds	$T_4 - T_{12} < 4.1$ or $\Delta T \geq 19$			
Eliminate highly reflecting clouds and surfaces	$\rho_2 \leq 0.22$	$\rho_2 \leq 0.25$		$\rho_2 \leq 16\%$
Eliminate sun glint		$\lvert\rho_1 - \rho_2\rvert > 0.01$		
Eliminate cropland or grassland false fire	Non-forest and isolated pixels	Maximum annual NDVI > 0.08		

ρ_1 and ρ_2 are the reflectances in band 1 (0.66 μm) and band 2 (0.86 μm) for AVHRR; T_4, T_{11} and T_{12} are the brightness temperature values in band 3 (3.75 μm), band 4 (10.8 μm) and band 5 (11.9 μm) for AVHRR; ΔT is $T_4 - T_{11}$, *NDVI* Normalized Difference Vegetation Index

and C6, respectively). Four prominent contextual fire algorithms are based on AVHRR, MODIS, VIIRS, and Landat 8.

A contextual method based on a fuel mask model of AVHRR

In the fuel mask model of fire detection, pixels were first tested for fuel availability according to pre-fire vegetation index values before identifying the potential fire pixels. A Normalized Difference Vegetation Index (NDVI) fuel mask algorithm was developed by Chuvieco and Martin (1994), who used the NDVI maximum value composite method within a 1-month compositing period. NDVI could be determined from the visible and near infrared channels of different sensors. A NDVI value was used as an additional initial threshold. It is assumed that only pixels with values greater than the NDVI threshold would be considered to have adequate fuel for maintaining a fire. This method could eliminate most of the false alarms caused by non-vegetative surfaces (Boles and Verbyla 2000). Many studies demonstrated that fire detection accuracy was improved by using a fuel mask model (Boles and Verbyla 2000; Chuvieco and Martin 1994; Zhou et al. 2006).

A contextual method based on the MODIS

Giglio et al. (2003) developed an enhanced contextual fire detection algorithm that was used for MODIS C4 FP. The MODIS C4 algorithm was based on the original MODIS contextual algorithm (Kaufman et al. 1998), but it offered superior sensitivity to smaller, cooler fires and achieved significantly lower false alarm rates. Compared with the MODIS C3 algorithm, MODIS C4 made two improvements by using several solar reflectance channels to reject false alarms and by adjusting the potential fire thresholds and contextual thresholds (Giglio et al. 2003).

The MODIS C4 algorithm assigned the MODIS imagery to six classes including missing data, cloud, water, non-fire, fire, and unknown, and its procedure consisted of the following stages (Giglio et al. 2003):

(1) *Cloud and water masking stage* Cloud and water pixels were identified and assigned to the classes of cloud and water, respectively. Water pixels were identified using the 1-km land/sea mask contained in the MODIS geolocation product. Cloud pixels were detected using a spectral profiling approach.

(2) *Identifying potential fire pixels (PFPs) stage* Obvious non-fire pixels were eliminated using preliminary tests: $T_4 > 310$ K and $\Delta T > 10$ K and $\rho_{0.86} < 0.3$ (where, $\rho_{0.86}$ is the reflectance of 0.86 μm channel) for daytime and $T_4 > 305$ K for nighttime.

(3) *Background characterization stage* The bright temperature of the PFPs in the absence of a fire was estimated by computing statistical summaries of valid background pixels (VBPs) within a background window surrounding the PFPs. VNPs were remaining clear land pixels after the exclusion of water, cloud and background fire pixels (BFPs) from PFPs (Giglio et al. 2003). BFPs were those that met the tests $T_4 > 325$ K and $\Delta T > 20$ K in daytime or $T_4 > 310$ K and $\Delta T > 10$ K in nighttime (Kaufman et al. 1998; Giglio et al. 2003).

(4) *Tentative fire detection stage* Contextual threshold tests were performed in series to derive the final identification for nighttime fires.

(5) *Cleaning stage* Sun glint, desert boundary, and coastal false alarm in daytime fires were rejected using additional steps.

Although the MODIS C4 and MODIS C5 algorithms functioned reasonably well, their performance was limited by two problems. First, smaller and cooler fires in some

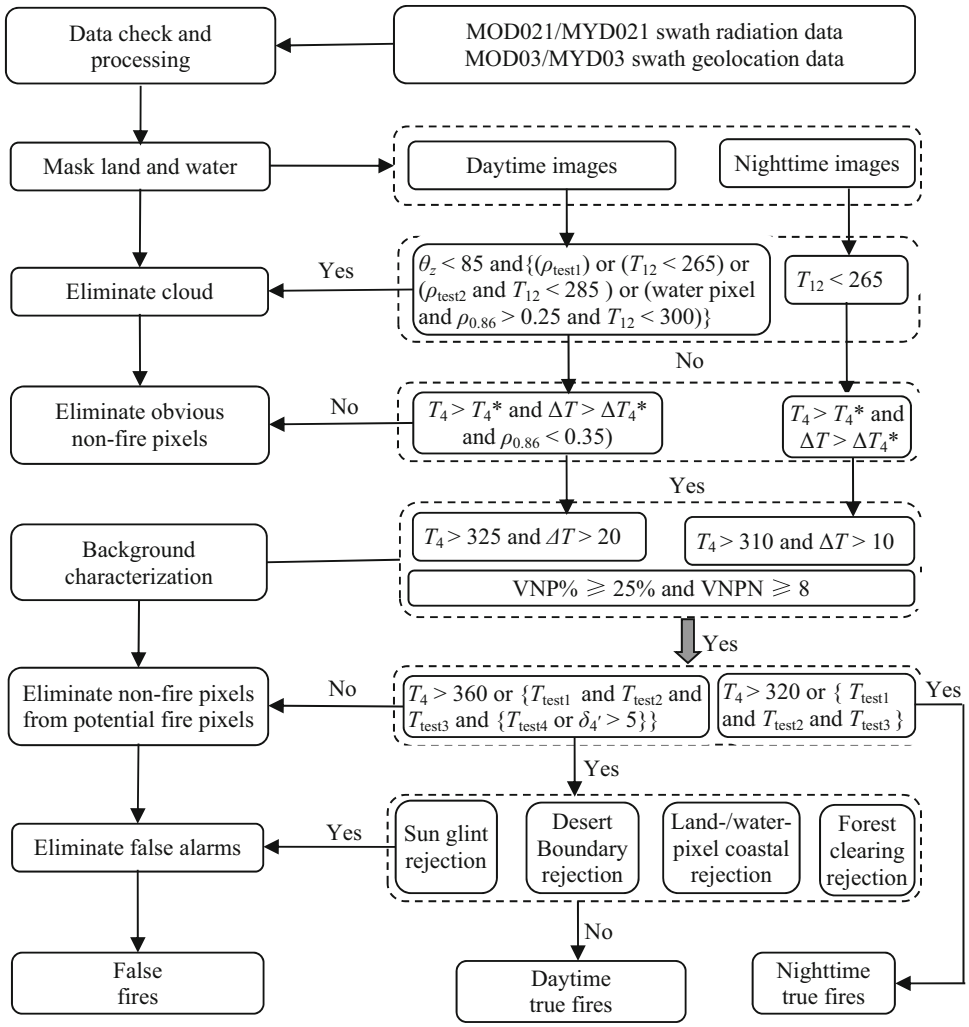

Fig. 3 An integrated framework for MODIS Collection 6 active fire algorithms (Giglio et al. 2016). θ_z is solar zenith angle; VNP% and VNPN are fraction valid background pixels (VBPs) and the numbers of VBPs in the neighborhood background window; ρ_{test1} and ρ_{test2} represent $\rho_{0.65} + \rho_{0.86} > 1.2$ and $\rho_{0.65} + \rho_{0.86} > 0.7$, respectively; T_{test1}, T_{test2}, T_{test3} and T_{test4} represent $\Delta T > \Delta T_B + 3.5\delta_{\Delta T}$, $\Delta T > \Delta T_B + 6$, $T_4 > T_{4B} + 3\delta_4$, and $T_{11} > T_{11B} + \delta_{11} - 4$, respectively; T_4, T_{11} and T_{12} represent brightness temperatures at MODIS 3.96-, 11.0- and 12.0 μm channels, respectively; $\rho_{0.65}$, $\rho_{0.86}$ represent the reflectance at MODIS 0.65-, and 0.86- μm channels, respectively; $\Delta T = T_4 - T_{11}$; T_4* and ΔT_4* are the 3.96-μm potential fire thresholds derived from a dynamic algorithm; T_{4B}, T_{11B}, and ΔT_B represent respective means of T_4, T_{11} and ΔT for VBPs; δ_4, δ_{11}, and $\delta_{\Delta T}$ represent respective mean absolute deviations of T_4, T_{11} and ΔT for VBPs; δ_4' is mean 3.96 μm bright temperature of pixels rejected as background fires. The unit of temperature is K

regions (Wang et al. 2007, 2009; Cheng et al. 2013) and large fires obscured by thick smoke (Schroeder et al. 2008) were frequently undetected. The main reason is that tests for detecting PFPs are absolute rather than dynamic thresholds. Second, false alarms often arise from small forest clearings (~1 km) within tropical rainforest.

In response to these problems, Giglio et al. (2016) developed a replacement contextual algorithm version 6 (Fig. 3). The MODIS C6 algorithm had the following enhancements: (1) water and land masking was realized by using the updated 1-km land/sea mask contained in the MODIS Collection 6 MOD03/MYD03 geolocation product; (2) cloud masking algorithm was improved to eliminate occasional misclassification of thick smoke as cloud; (3) potential fire thresholds were adaptively assigned to better capture small, cool fires and reduce false alarms occurring in hot, arid environments; Instead of fixed PFPs thresholds in the previous algorithms, it set dynamic thresholds ($T_4 > \text{mean}\ (T_4)_j + 5$ K, $\Delta T > \text{mean}\ (\Delta T)_j + 5$ K) for each of the 1354 sample positions of the current MODIS scan by averaging the values of T_4 and ΔT for all cloud- and glint-free land pixels within a large, 301-sample by 30-line moving window centered upon sample position j ($0 \le j \le 1{,}353$). This along-scan adjusting compensated for local variations in the land surface as well as the systematic increase in atmospheric path length with scan angle;

(4) a new rejection test was executed to greatly reduce false alarms in the tropical rainforest regions caused by small forest clearings; (5) processing of water pixels was extended to facilitate monitoring of offshore gas flaring; (6) fire detection confidence calculation was slightly adjusted.

A contextual method based on VIIRS

Two algorithms were developed with VIIRS 750 m data. One was based on the MODIS C4 fire algorithm (Giglio et al. 2003) and used for the operational VIIRS 750 m Active Fires Application Related Product. The other was based on the VIIRS 750 m 1.61 μm channel and Day-Night Band data to detect gas flares and other high temperature sources at night (Elvidge et al. 2013).

For VIIRS 375 m data, a contextual algorithm was proposed by Schroeder et al. (2014) on the basis of the well-established MODIS fire and thermal anomalies, which underwent several years of algorithm development, validation and refinement (Kaufman et al. 1998; Giglio et al. 2003; Schroeder et al. 2008). VIIRS 375 m data are comprised of five distinct single-gain channels extending from the visible to thermal infrared spectral regions. Improved spatial resolution could help detect smaller fires of the same temperature, as well as refine mapping of larger fires, which would further help fire management and related research (Schroeder et al. 2014). However, the VIIRS 375 m data have a lower saturation temperature (367 K) in the MIR channel than do VIIRS 750 (634 K) and MODIS (500 K) data, which, in combination with the improved spatial resolution, can result in frequent fire pixel saturation.

Compared with the MODIS C4 algorithm, the VIIRS 375 m algorithm has four major features: (1) water pixels were eliminated for daytime using a spectral profiling approach rather than by an internal sea/land mask; (2) potential fire pixels were identified to eliminate obvious non-fire pixels by using the tests: $T_{MIR} > T_s$ or $\Delta T > 25$ in daytime or $T_{MIR} > 295$ or $\Delta T > 10$ at night (where, T_s was a large area background brightness temperature reference value on the MIR channel, i.e., I4) (Table 1), which was calculated for a 501 × 501 window centered on the candidate fire pixels. The large-area background sampling scheme accommodated variations in background conditions and helped capture fires occurring in colder high latitude regions and reduced false alarm rates in lower latitudes where backgrounds were warmer; (3) in background characterization stage, the background window size could vary from 11 × 11 to 31 × 31 pixels until at least 25% of the sample size consisted of valid pixels, or a minimum of 10 valid pixels were found; (4) daytime sun glint, bright targets (such as sand) false alarm, and nighttime South Atlantic Magnetic Anomaly false alarms were rejected.

A contextual method based on Landsat 8 OLI

Schroeder et al. (2016) developed a new active fire algorithm for Landsat-8 OLI on the basis of the ASTER (Giglio et al. 2008) and Landsat-7/ETM + algorithms. It incorporated additional visible and near-infrared channel data and a multi-temporal analysis scheme. For nighttime scenes, a single band 7 radiance threshold test was performed. For daytime scenes, the algorithm involved mainly the following stages: (1) Water pixels were eliminated based on spectral profiling approach using reflectance data from all seven input channels; (2) Obvious fire pixels were identified based on simple fixed thresholds. The pixels were directly classified as fire pixels and exempted from the contextual fire detection analysis; (3) Candidate fire pixels were identified to eliminate obvious non-fire pixels by using the tests: $r > 1.8$ and $\Delta\rho > 0.3$ and $\rho_7 > 0.17$ (where, r is the ratio of channel 7 to channel 5 ($r = \rho_7/\rho_5$), and $\Delta\rho$ is the difference of channel 7 and 5 reflectance values ($\Delta\rho = \rho_7 - \rho_5$)); (4) In background characterization stage, the size of background window is fixed at 61 × 61 pixels (i.e., 1,830 × 1,830 m) rather than variable window sizes used in some coarser resolution (1 km) sensors; (5) All candidate fire pixels were further processed by using three contextual tests; (6) A multi-temporal analysis was conducted to eliminate false alarms caused by urban environments or exposed soils under specific illumination conditions.

The Landsat-8 algorithm resulted in a 30 m active FP, which generated more information per unit area than did VIIRS 375 m or MODIS (1 km) but was limited by small coverage of each scene and a low revisit cycle of 16 days. Nevertheless, such a 30 m algorithm shows great potential because launches of other similar sensors can greatly increase data availability (Schroeder et al. 2016).

Multi-temporal methods

The multi-temporal fire detection methods focus on exploiting the multi-temporal nature of data in a thermal anomaly detection process. The major multi-temporal fire detection algorithms included non-linear dynamic detection model (Koltunov and Ustin 2007), multi-temporal Kalman filter approach (Roberts and Wooster 2014), spatiotemporal model (Lin et al. 2016), and RST-FIRES (Mazzeo et al. 2007; Filizzola et al. 2016).

Filizzola et al. (2016) provided detailed descriptions of the algorithm of RST-FIRES, which adopted a series of thermal indices derived from a general Absolutely Local Index of Change of Environment (ALICE) index. The thermal indices consisted of ALICE intensity (Eq. 5), spectral ALICE, time differential ALICE, and space differential ALICE.

$$\otimes_{\mathrm{MIR}}(x,y,t) = \frac{T_{\mathrm{MIR}}(x,y,t) - \mu_{\mathrm{MIR}}(x,y)}{\sigma_{\mathrm{MIR}}(x,y)} \quad (5)$$

where, $T_{\mathrm{MIR}}(x, y, t)$ is the brightness temperature measured in the MIR channel of the sensor at (x, y) location and time t; μ_{MIR} (x, y) and σ_{MIR} (x, y), so-called 'reference fields', are the temporal mean and the standard deviation of T_{MIR} (x, y, t) computed at the same place (x, y) using long-term multi-temporal cloud-free satellite records. The reference fields represent the expected values of thermal signals in 'normal' or unperturbed conditions and their statistical fluctuations.

In the RST-FIRES method, fires were categorized into extreme starting, starting, ongoing, possible starting, and possible ongoing fires according to their development stages and probabilities of occurrence. The five types of fires could be detected by using a series of different combinations tests of the four RST-based indices. Therefore, RST-FIRES not only accurately detected fire pixels but also discriminated them on the basis of fire extension or intensity.

The RST-FIRES algorithm is effective with satellite data acquired in different areas, under different conditions, and with different sensors onboard either polar (Mazzeo et al. 2007) or geostationary platforms (Filizzola et al. 2016). However, the application of the approach to the geostationary sensors yields greater advantage than onboard polar sensors because of its uniquely high revisit cycles. Its disadvantage is that it requires many time-series cloud-free and unperturbed images, at least 80 per month (Koeppen et al. 2011), to compute the reference fields. Clouds can indirectly affect RST-FIRES performance since they reduce the reliability of computed reference values for temporal average and standard deviation.

Drone IRRS methods

Merino et al. (2012) presented a drone-based perception system for FFM, which involved multiple drones and a ground central station (Fig. 4). Each drone was equipped with a decisional system (i.e., inertial measurement units and global positioning systems) and a perception system (i.e., infrared and visual cameras). The mission of the drones included fire search, localization, and monitoring. The decisional system was for the tasks of allocation, planning, synchronization, and supervision between drones in a decentralized manner. The perception system considered all the information gathered by the different drones to estimate the evolution of the fire by applying data fusion techniques. In the perception system, each drone could locally process its images and provide features related to the fire front evolution. The onboard communication devices carried by drones were able to receive commands from the ground station, and to send information back to it. All the data from the drones were sent to the central station, where they were integrated to estimate real-time evolution of the fire.

Typical cases of FFM with IRRS

NOAA-AVHRR applications

Flannigan and Haar (1986) used the Dozier bi-spectral technique and AVHRR data to monitor forest fires in north central Alberta, Canada. In the absence of cloud and smoke cover, their approach identified 80% of fire observations reported on the ground. In addition, they identified sub-pixel fires as small as 1 ha.

Li et al. (2000) developed a multi-channel algorithm for FFM in boreal forest ecosystems, which was later adopted by the Canada Centre for Remote Sensing (CCRS). They provided the first comprehensive satellite surveillance of forest fires across Canada using the AVHRR daily imagery data acquired in 1994–1997. The results provided valuable nation-wide information on fire locations, burned area, starting and ending dates, and fire development.

Since the CCRS algorithm was designed for fire detection in Canadian boreal forests with a "cold background", it could not be applied directly to forests with "warm background" in California, USA (Li et al. 2003). Gong et al. (2006) developed an improved CCRS approach to map wildfires in California, which eliminated the false alarms from warm backgrounds such as bare soil, and sun glint problem caused by the coastline and many inner lakes in California. The wildfire mapping using the new approach proved largely correct, especially for those fires in forested ecosystems.

EOS-Modis applications

Urbanski et al. (2009) evaluated the MODIS C4 algorithm's fire detection rate using fire perimeter data derived from AVHRR in western United States. The study showed that the fire detection rate increased with fire size. The algorithm detected 87% of reference fires >4 km^2 and but only 19% of reference fires <1 km^2. For coniferous-forest, grassland and shrubland fires >2 km^2, the detection rates were 100, 75, and 70%, respectively. But these detection rates declined to 65, 28, and 16% when fire extents were $\leq$2 km^2. This demonstrated that the MODIS C4 algorithm was more effective at detecting forest fires compared with grassland and shrubland fires.

The MODIS C4 algorithm was designed for operational global fire monitoring and had limitations for regional fire detection. One important reason is that the preliminary PFP

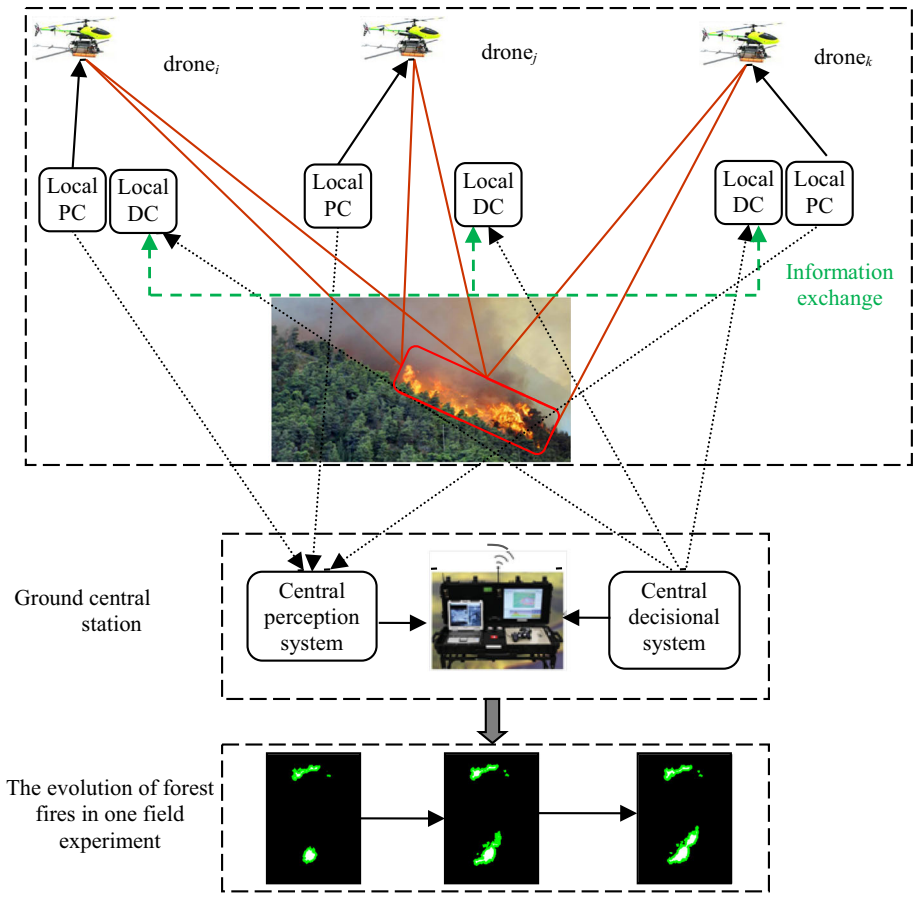

Fig. 4 The system components and conception for drone-based forest fire monitoring (Merino et al. 2012; Yuan et al. 2015). *PC* perception component, *DC* decisional component

thresholds can be set low enough to detect very small fires. A number of case studies demonstrated that the MODIS C4 algorithm often omitted the smaller and cooler fires. Wang et al. (2007) and Wang et al. (2009) used the MODIS C4 algorithm to detect fires in southeastern United States, where small and cool fires were dominant. A large fraction of small fire pixels that had 4-μm brightness temperatures below the 310 K daytime potential fire threshold (i.e., $T_4 < 310$ K) were not detected. They proposed an improved algorithm by combining the MODIS C4 and a smoke detection algorithm, and increased the capability to detect small and cool fires. Cheng et al. (2013) used the MODIS C4 method in a subtropical Yucatán forest. Their experiments showed that only 23% of forest fires were detected because the 310 K MODIS 4-μm threshold was higher than the temperature of most forest fires.

Giglio et al. (2016) compared MODIS C5 and C6 by using reference fire maps derived from more than 2500 high-resolution ASTER images. At the global scale, MODIS C6 daytime data resulted in a commission error of 1.2% whereas C5 data caused 2.4% commission error. At the regional scale, the C6 data yielded an increase of 1–3% in the fire detection rate in most regions. More importantly, C6 data significantly reduced false alarm rates compared to C5 data in high forest cover regions, particularly in tropical forests. Such improvements in performance were contributed by the forest clearing rejection test, dynamic thermal potential fire thresholds, and increased 0.86-μm reflectance threshold, which reduced both commission errors from small forest clearings and omission errors from thick smoke.

Peterson et al. (2013) developed an improved bi-spectral method by combining the previous bi-spectral retrievals with a radiative transfer model. The retrieved sub-pixel fire (flaming) area was assessed via multispectral, high-resolution data (3-50 m) obtained from the Autonomous Modular Sensor (AMS), flown aboard the NASA Ikhana drone. With fire sizes ranging from 0.1 to 2 ha, pixel-level fire area comparisons between MODIS and AMS showed a modest correlation ($R = 0.59$). The correlation became much stronger ($R = 0.84$) when lower confidence fire pixels were removed. The highest correlation ($R = 0.91$) was produced with a comparison method based on cluster-level fire area created by adjacent hotspot pixels. The pixel clustering analysis suggested that the random variation could be reduced by averaging when looking at a fire event as a whole.

S-NPP VIIRS applications

Oliva and Schroeder (2015) evaluated the performance of the VIIRS 375 m active FP (VIIRS375-AFD) for direct burned area mapping in ten regions with distinct fire-prone ecosystems around the world. The fire detection rate was defined as the ratio of the VIIRS 375 m burned areas (VIIRS375-BAs) to the reference (i.e., Landsat-8 burned area patches). The VIIRS375-BAs were estimated by directly aggregating consecutive VIIRS375-AFD instead of a complex image classification approach. VIIRS375-AFD accurately identified >80% of fires covering over 10 ha in boreal, mixed temperate or Mediterranean forests. The study demonstrated the improved sensitivity of the VIIRS 375-AFD algorithm to small active fires. It also indicated VIIRS375-AFD could be used for routine mapping of burned area based on cumulative fire count or seeding of spectral signatures.

When the VIIRS 375 m fire data were applied to monitor the growth of long-lasting wildfires in California in 2013, its performance showed high agreement with available fine resolution nighttime thermal airborne data, overestimating only 10-20% of the total burned area. This application demonstrated that the VIIRS375-BAs data could serve as an alternative means to monitor large fire growth.

Landsat 8 OLI applications

The Landsat-8 OLI algorithm was evaluated with a great number of global fire data via visual inspection and field experiment (Schroeder et al. 2016). The fire data for visual inspection were derived from publicly available data sources including high spatial resolution imagery. The overall commission errors of daytime fire detections were <0.2% globally, and the error for nighttime was negligible. Because of multi-temporal analysis tests used in the algorithm, commission errors were greatly reduced. The algorithm showed significant improvement in performance for detecting small fires and delineating large wildfires compared to the existing operational satellite FPs with coarser spatial resolution. The OLI-based active fire measurements could become an important part of the international network for FFM in the future (Loveland and Irons 2016).

MSG-SEVIRI applications

Mazzeo et al. (2007) applied RST-FIRES to monitor important forest fires in northern Italy by using AVHRR and SEVIRI data. This study pointed out that the approach did not require any ancillary information and thus could easily be implemented on whatever satellite platform to monitor forest fires at the global scale, in particular for SEVIRI data due to high temporal resolution. This technique could be used in various observational conditions (day/night, summer/winter) without significant difference in reliability, being insensitive to reflected solar radiation effects by bare soil and the variation of surface emissivity.

Filizzola et al. (2016) assessed the performances of the RST-FIRES technique to identify fire events in two Italian regions with more than 20,000 SEVIRI images acquired in 268 days between 2009 and 2015. A systematic field check was carried out with 950 near real-time ground and aerial observations. The results showed that the RST-FIRES technique had a false alarm rate (i.e., commission error) of 18% (3–30%), and had an average omission error of 44% (3–66%). The RST-FIRES also provided the sole fire alert in 348 cases that would not be documented in official reports owing to their nature or short duration. It gave >1 h warning prior to any other information sources from ground or aerial checks in a further 227 cases. The study fully demonstrated the great capability (added value) of the RST-FIRES technique for the early warning of fire events.

Drones IRRS applications

Ambrosia et al. (2011) reported that NASA and the US Forest Service used large, long-duration, fixed-wing drones to perform 57 fire imaging missions in western United States between 2006 and 2010. The study demonstrated that the fixed-wing drone platform could play a significant role in providing near-real-time (5–10 min) intelligence to assist forest wildfire control and management.

Merino et al. (2012) tested the ability of a system based on multiple rotary-wing drones to monitor forest wildfires by a variety of near-operational experiments in Spain and Portugal. The study showed that the multiple drones system was effective for obtaining real-time data of forest wildfires. Furthermore, the multiple drones could collaboratively monitor larger areas of forest fires by obtaining complementary views of wildfires.

Concluding remarks

The utilization of forest masks can help greatly improve forest fire detection accuracy. In other words, it is critical to monitor forest fires through the integration of the existing fire monitoring algorithms with forest masks. However, the NDVI-based masks that have frequently been used might not distinguish forests from other vegetation types. Therefore, more accurate approaches for extracting forests need to be developed and integrated into fire monitoring algorithms to better forecast, detect and monitor forest fires.

The algorithms of active fire detections with various sensors are increasingly mature and rapidly advancing from simple to complex spatial contextual methods. The detection rates of small and cool fires have also been significantly improved as the fire algorithms (e.g., MODIS C4 to MODIS C6) were improved and satellite data at finer spatial resolution became increasingly available. Due to high spatiotemporal resolutions of VIIRS375-AFD, more attention is expected to the mapping of routine burned areas and continuous monitoring of large-scale fire growth in near real time. As high spatial resolution active fire data (e.g., Landsat 8 OLI) emerge, they will foster the development in new applications of landscape-scale fire analysis, such as forest fire growth evaluation and tactical fire management (Schroeder et al. 2016). As multi-temporal fire algorithms (e.g., RST-FIRES) were applied to geostationary sensor data, in particularly for SEVIRI, they can play more roles in timely detection of forest fires, including small or short-lived events at very early stages, and providing early warnings, owing to their very high temporal resolution. Most of the existing research on FFM by the use of drones was carried out either in laboratory or near-operational environments. This research is expected to expand rapidly (Merino et al. 2012; Yuan et al. 2015) because drones of various shapes and functions are rapidly emerging and their corresponding FFM algorithms will become more mature in future.

At present, a great number of IRRS algorithms have been employed to generate FPs with various spatial (30 m to 3 km) and temporal resolutions (minutes to days). Some FPs are still relatively new and have been tested only over small areas. Examples are those derived from Landsat 8 OLI and VIIRS 375 m. It is important to develop more FPs from different sensors over important regions around the world. Additional efforts will be made to compare and evaluate the performance of these FPs with new assessment methods that can consider the dynamic nature of forest fires.

References

Ahmad AAA (2014) A review on forest fire detection techniques. Int J Distrib Sensor Netw 10(3):1–12

Ambrosia V, Wegener S, Zajkowski T, Sullivan D, Buechel S, Enomoto F, Lobitz B, Johan S, Brass J, Hinkley E (2011) The Ikhana unmanned airborne system (UAS) western states fire imaging missions: from concept to reality (2006–2010). Geocarto Int 26(2):85–101

Andreae MO (2013) Magnitude and impacts of vegetation fire emissions on the atmosphere. In: Goldammer JG (ed) Vegetation fires and global change: challenges for concerted international action: a white paper directed to the United Nations and International Organizations. Kessel Publishing House, Remagen, pp 171–180

Arino O, Melinotte JM (1998) The 1993 Africa fire map. Int J Remote Sens 19(11):2019–2023

Arino O, Rosaz JM (1999) 1997 and 1998 World ATSR Fire Atlas using ERS-2 ATSR-2 data. In: Neuenschwander LF, Ryan KC, Golberg GE (eds) Proceedings of the joint fire science conference. University of Idaho and the International Association of Wildland Fire, Boise, pp 177–182

Blackett M (2015) An initial comparison of the thermal anomaly detection products of MODIS and VIIRS in their observation of Indonesian volcanic activity. Remote Sens Environ 171:75–82

Boles SH, Verbyla DL (2000) Comparison of three AVHRR-based fire detection algorithms for interior Alaska. Remote Sens Environ 72(1):1–16

Calle A, Casanova JL (2008) Forest fires and remote sensing. In: Coskun HG, Cigizoglu HK, Maktav MD (eds) Integration of information for environmental security. Springer, Berlin, pp 247–290

Cao CY, De Luccia FJ, Xiong XX, Wolfe R, Weng FZ (2014) Early on-orbit performance of the visible infrared imaging radiometer suite onboard the suomi national polar-orbiting partnership (S-NPP) satellite. IEEE Trans Geosci Remote 52(2):1142–1156

Cheng D, Rogan J, Schneider L, Cochrane M (2013) Evaluating MODIS active fire products in subtropical Yucatán forest. Remote Sens Lett 4(10):455–464

Chuvieco E, Martin MP (1994) A simple method for fire growth mapping using AVHRR channel 3 data. Int J Remote Sens 15(16):3141–3146

Csiszar I, Schroeder W, Giglio L, Ellicott E, Vadrevu KP, Justice CO, Wind B (2014) Active fires from the Suomi NPP visible infrared imaging radiometer suite: product status and first evaluation results. J Geophys Res 119(2):803–816

Cuomo V, Lasaponara R, Tramutoli V (2001) Evaluation of a new satellite-based method for forest fire detection. Int J Remote Sens 22(9):1799–1826

Dennison PE, Brewer SC, Arnold JD, Moritz MA (2014) Large wildfire trends in the western United States, 1984–2011. Geophy Res Lett 41(8):2928–2933

Dozier J (1981) A method for satellite identification of surface temperature fields of subpixel resolution. Remote Sens Environ 11:221–229

Eckmann TC, Roberts DA, Still CJ (2008) Using multiple endmember spectral mixture analysis to retrieve subpixel fire properties from MODIS. Remote Sens Environ 112:3773–3783

Elvidge CD, Zhizhin M, Hsu FC, Baugh KE (2013) VIIRS nightfire: satellite pyrometry at night. Remote Sens 5(9):4423–4449

Filizzola C, Corrado R, Marchese F, Mazzeo G, Paciello R, Pergola N, Tramutoli V (2016) RST-FIRES, an exportable algorithm for early-fire detection and monitoring: description, implementation, and field validation in the case of the MSG-SEVIRI sensor. Remote Sens Environ 186:196–216

Flannigan MD, Haar THV (1986) Forest fire monitoring using NOAA satellite AVHRR. Canadian J Forest Res 16(5):975–982

Giglio L, Kendall JD (2001) Application of the Dozier retrieval to wildfire characterization: a sensitivity analysis. Remote Sens Environ 77(1):34–49

Giglio L, Schroeder W (2014) A global feasibility assessment of the bi-spectral fire temperature and area retrieval using MODIS data. Remote Sens Environ 152:166–173

Giglio L, Kendall JD, Justice CO (1999) Evaluation of global fire detection algorithms using simulated AVHRR infrared data. Int J Remote Sens 20(10):1947–1985

Giglio L, Descloitres J, Justice CO, Kaufman YJ (2003) An enhanced contextual fire detection algorithm for MODIS. Remote Sens Environ 87(2):273–282

Giglio L, Csiszar I, Justice CO (2006) Global distribution and seasonality of active fires as observed with the Terra and Aqua Moderate Resolution Imaging Spectroradiometer (MODIS) sensors. J Geophys Res 111(G2):1–12

Giglio L, Csiszar I, Restás Á, Morisette JT, Schroeder W, Morton D, Justice CO (2008) Active fire detection and characterization with the advanced spaceborne thermal emission and reflection radiometer (ASTER). Remote Sens Environ 112(6):3055–3063

Giglio L, Schroeder W, Justice CO (2016) The collection 6 MODIS active fire detection algorithm and fire products. Remote Sens Environ 178:31–41

Gong P, Pu R, Li Z, Scarborough J, Clinton N, Levien LM (2006) An integrated approach to wildland fire mapping of California, USA using NOAA/AVHRR data. Photogramm Eng Remote Sens 72(2):139–150

Kaufman YJ, Tucker CJ, Fung I (1990) Remote sensing of biomass burning in the tropics. J Geophys Res 95(D7):9927–9939

Kaufman YJ, Justice C, Flynn L (1998) Monitoring global fires from EOS-MODIS. J Geophys Res 102(29):611–624

Kennedy PJ, Belward AS, Gregoire JM (1994) An improved approach to fire monitoring in West Africa using AVHRR data. Int J Remote Sens 15(11):2235–2255

Koeppen W, Pilger E, Wright R (2011) Time series analysis of low resolution thermal infrared satellite data for detecting thermal anomalies: a hybrid approach. Bull Volcanol 73(5):577–593

Koltunov A, Ustin SL (2007) Early fire detection using non-linear multitemporal prediction of thermal imagery. Remote Sens Environ 110(1):18–28

Langaas S (1992) Temporal and spatial distribution of Savannah fires in Senegal and the Gambia, West Africa, 1989–1990, derived from multi-temporal AVHRR night images. Int J Wildland Fire 2(1):21–36

Lavrov A, Utkin AB, Vilar R, Fernandes A (2006) Evaluation of smoke dispersion from forest fire plumes using lidar experiments and modeling. Int J Therm Sci 45(9):848–859

Li Z, Nadon S, Cihlar J (2000) Satellite-based detection of Canadian boreal forest fires: development and application of the algorithm. Int J Remote Sens 21(16):3057–3069

Li X, Kaufman YJ, Ichoku C, Fraser R, Trishcenko A, Giglio L, Kin J, Yu X (2001) A review of AVHRR-based active fire detection algorithms: principles, limitations, and recommendations. In: Ahern FJ, Goldammer JG, Justice CO (eds) Global and regional vegetation fire monitoring from space: planning and coordinated international effort. SPB Academic, Hague, pp 199–225

Li ZQ, Fraser R, Jin J, Abuelgasim AA, Csiszar I, Gong P, Pu R, Hao W (2003) Evaluation of algorithms for fire detection and mapping across North America from satellite. J Geophys Res 108(D2):171–181

Li XL, Song WG, Lian LP, Wei XG (2015) Forest fire smoke detection using back-propagation neural network based on MODIS data. Remote Sens 7(4):4473–4498

Lin L, Meng Y, Yue AZ, Yuan Y, Liu XY, Chen JB, Zhang MM, Chen JS (2016) A spatio-temporal model for forest fire detection using HJ-IRS satellite data. Remote Sens 8(5):403

Loveland TR, Irons JR (2016) Landsat 8: the plans, the reality, and the legacy. Remote Sens Environ 185:1–6

Martell DL (2015) A review of recent forest and wildland fire management decision support systems research. Curr For Rep 1(2):128–137

Matson M, Dozier J (1981) Identification of subresolution high temperature sources using a thermal IR sensor. Photogramm Eng Remote Sens 47(9):1311–1318

Mazzeo G, Marchese F, Filizzola C, Pergola N, Tramutoli V (2007) A multi-temporal robust satellite technique (RST) for forest fire detection. In: Proceedings of the international workshop on the analysis of multi-temporal remote sensing images. IEEE, Piscataway. Doi: 10.1109/MULTITEMP.2007.4293060

Meng Y, Deng Y, Shi P (2015) Mapping forest wildfire risk of the world. In: Shi PJ, Kasperson R (eds) World atlas of natural disaster risk. Springer, Berlin, pp 261–275

Merino L, Caballero F, Martrial de Dios R, Maza I, Ollero A (2012) An unmanned aircraft system for automatic forest fire monitoring and measurement. J Intell Robot Syst 65(1):533–548

Oliva P, Schroeder W (2015) Assessment of VIIRS 375 m active fire detection product for direct burned area mapping. Remote Sens Environ 160:144–155

Ollero A, Merino L (2006) Unmanned aerial vehicles as tools for forest-fire fighting. For Ecol Manag 234(1):S263

Peterson D, Wang J, Ichoku C, Hyer E, Ambrosia V (2013) A sub-pixel-based calculation of fire radiative power from MODIS observations: 1: algorithm development and initial assessment. Remote Sens Environ 129:262–279

Pozo D, Olrno FJ, Alados-Arboledas L (1997) Fire detection and growth monitoring using a multitemporal technique on AVHRR mid-infrared and thermal channels. Remote Sens Environ 60(2):111–120

Pu RL, Gong P, Li ZS, Scarborough J (2004) A dynamic algorithm for wildfire mapping with NOAA/AVHRR data. Int J Wildland Fire 13(3):275–285

Qu JJ, Wang W, Dasgupta S, Hao X (2008) Active fire monitoring and fire danger potential detection from space: a review. Front Earth Sci in Chin 2(4):479–486

Roberts GJ, Wooster MJ (2008) Fire detection and fire characterization over Africa using Meteosat SEVIRI. IEEE Trans Geosci Remote 46(4):1200–1218

Roberts G, Wooster MJ (2014) Development of a multi-temporal Kalman filter approach to geostationary active fire detection & fire radiative power (FRP) estimation. Remote Sens Environ 152:392–412

Roy DP, Boschetti L, Justice CO, Ju J (2008) The collection 5 MODIS burned area product—global evaluation by comparison with the MODIS active fire product. Remote Sens Environ 112:3690–3707

Sahin YG, Ince T (2009) Early forest fire detection using radio-acoustic sounding system. Sensors 9(3):1485–1498

San-Miguel-Ayanz J, Ravail N (2005) Active fire detection for fire emergency management: potential and limitations for the operational use of remote sensing. Nat Hazards 35(3):361–376

Schroeder W, Prins E, Giglio L, Csiszar I, Schmidt C, Morisette JT, Morton D (2008) Validation of GOES and MODIS active fire detection products using ASTER and ETM+ data. Remote Sens Environ 112:2711–2726

Schroeder W, Oliva P, Giglio L, Csiszar IA (2014) The New VIIRS 375 m active fire detection data product: algorithm description and initial assessment. Remote Sens Environ 143:85–96

Schroeder W, Oliva P, Giglio L, Quayle B, Lorenz E, Morelli F (2016) Active fire detection using Landsat-8/OLI data. Remote Sens Environ 185:210–220

Setzer AW, Pereira MC (1991) Amazonian biomass burnings in 1987 and an estimate of their tropospheric emission. Ambio 20(1):19–22

Shao GF (2015) Optical remote sensing. In: Richardson D (ed) The international encyclopedia of geography: people, the earth, environment, and technology, 2nd edn. Wiley, Chichester, pp 2390–2395

Tang LN, Shao GF (2015) Drone remote sensing for forestry research and practices. J For Res 26(4):791–797

Urbanski SP, Salmon JM, Nordgren BL, Hao WM (2009) A MODIS direct broadcast algorithm for mapping wildfire burned area in the western United States. Remote Sens Environ 113(11):2511–2526

Vadrevu KP, Lasko K, Giglio L, Justice C (2015) Vegetation fires, absorbing aerosols and smoke plume characteristics in diverse biomass burning regions of Asia. Environ Res Lett 10:105003

Wang W, Qu JJ, Hao X, Liu Y, Sommers WT (2007) An improved algorithm for small and cool fire detection using MODIS data: a

preliminary study in the southeastern United States. Remote Sens Environ 108(2):163–170

Wang W, Qu JJ, Hao X, Liu Y (2009) Analysis of the moderate resolution imaging spectroradiometer contextual algorithm for small fire detection. J Appl Remote Sens 3(1):117–124

Weaver JF, Purdom JFW, Schneider TL (1995) Observing forest fires with the GOES-8, 3.9-μm imaging channel. Weather Forecast 10(4):803–808

Yuan C, Zhang YM, Liu ZX (2015) A survey on technologies for automatic forest fire monitoring, detection, and fighting using unmanned aerial vehicles and remote sensing techniques. Can J For Res 45(7):783–792

Zhou XC, Wang XQ, Xiang TL, Jiang H (2006) Validation analysis of the algorithm for identifying forest fire based on MODIS data. Fire Saf Sci 15(1):31–37 **(In Chinese)**

Zhukov B, Lorenz E, Oertel D, Wooster M, Roberts G (2006) Spaceborne detection and characterization of fires during the bi-spectral infrared detection (BIRD) experimental small satellite mission (2001–2004). Remote Sens Environ 100(1):29–51